Supporting Information

Unipolar electron transport polymers: A thiazole based all electron acceptor approach

Zhibo Yuan[1+], Boyi Fu[2+⊥], Simil Thomas[3], Siyuan Zhang[1], Giovanni DeLuca[1], Rui Chang[2], Lauren Lopez[2], Chaker Fares[2], Guoyan Zhang[2], Jean-Luc Bredas[3*], and Elsa Reichmanis[1, 2, 4]*

[1]*School of Chemistry and Biochemistry, Georgia Institute of Technology, 901 Atlantic Dr, Atlanta, GA 30332.*

[2]*School of Chemical and Biomolecular Engineering, Georgia Institute of Technology, 311 Ferst Dr NW, Atlanta, GA 30332.*

[3]*Laboratory for Computational and Theoretical Chemistry of Advanced Materials, Division of Physical Science and Engineering, King Abdullah University of Science and Technology, Thuwal 23955-6900, Kingdom of Saudi Arabia.*

[4]*School of Material Science and Engineering, Georgia Institute of Technology, 771 Ferst Dr NW, Atlanta, GA 30332.*

[+] *These authors contributed equally.*

[⊥] *Present Address: Applied Materials, Inc., 3050 Bowers Ave, Santa Clara, CA 95054 USA.*

Table of the Contents

Measurements and general methods:

Chloroform, dichloromethane, toluene, p-xylene (PX), isopropanol, tetrahydrofuran (THF), dimethylformamide (DMF), chlorobenzene and 1,2-dichorobenzene (o-DCB) were purchased as anhydrous grade solvents from Sigma-Aldrich. THF was distilled from sodium benzophenone in an solvent purification system (SPS). 2-Bromothiazole was purchased from Scientific Matrix. Tetrabutylammonium bromide (n-Bu4NBr), n,n-diisopropylethylamine (DIPEA), diisopropylamine (DIPA), palladium(II) acetate ($Pd(OAc)_2$), tris(dibenzylideneacetone)- dipalladium(0) ($Pd_2(dba)_3$), tri(o-tolyl)phosphine ($P(o\text{-tolyl})_3$), sodium diethyldithiocarbmate, and tetra-*n*-butylammonium hexafluorophosphate ([*n*-Bu_4N]+[PF_6]-) were purchased from Sigma-Aldrich. *N*-octadecyltrichlorosilane (OTS-18) was purchased from Gelest, Inc. Silica gel was purchased from Sorbent Technologies (Premium Rf™, porosity: 60A; particle size: 40-75 μm). UV-vis absorption spectra were recorded on an Agilent 8453 UV-Visible Spectrophotometer. **PDPP4Tz** films for UV-vis absorption characterization were prepared by spin-coating polymer solutions in p-xylene (5 mg/mL) and chloroform (5 mg/mL) onto pristine SiO_2 glass substrates and OTS-18 pre-treated glass cover substrates. The details of OTS-18 pretreatment are depicted in the section on "OFET Device Fabrication and Characterization".

The polymer thermal decomposition temperature was measured with a Perkin-Elmer Pyris-1 thermogravimetric analyzer (TGA) in a nitrogen atmosphere (25 mL/min) with a heating rate of 10 °C/min. Polymer thermal transitions were measured with a TA Q200 Differential Scanning Calorimeter (DSC) in a nitrogen atmosphere (50 mL/min) with a heating/cooling rate of 10 °C/min. Each sample was scanned for three cycles.

The surface morphologies of **PDPP4Tz** films were characterized by Atomic Force Microscopy (AFM) using a Bruker Dimension Icon Atomic Force Microscope System with ScanAsyst in the tapping mode using a silicon etched probe tip (Mikromasch USA, HQ:NSC14/NO AL). Polymer films for AFM characterization were prepared by spin-coating **PDPP4Tz** solutions in chloroform (5 mg/mL) and *p*-xylene (4 mg/mL) onto OTS-18 pre-treated SiO_2 dielectric (300 nm) / p++ doped Si substrates.

PDPP4Tz thin-film thermal annealing treatment was conducted on a hotplate with temperature setting of 150 °C inside a glovebox filled with N_2. Each thermal annealing treatment lasted for 90 min, followed by rapid cooling to room temperature. This annealing protocol was used for UV/vis absorption, 2D-GIWAXS, and AFM characterization.

Synthesis and characterization:

The synthetic procedures for the preparation of the 5-decylheptadecyl bromide side chains (**1a-1e**), 5,5'-bis(trimethylstannyl)-2,2'-bithiazole (**2c**), and 2,5-bis(5-decylheptadecyl)-3,6-di(thiazole-2-yl)pyrrolo[3,4-c]pyrrole-1,4(2H,5H)-dione (**3d**) were modified from literature procedures[1-3].

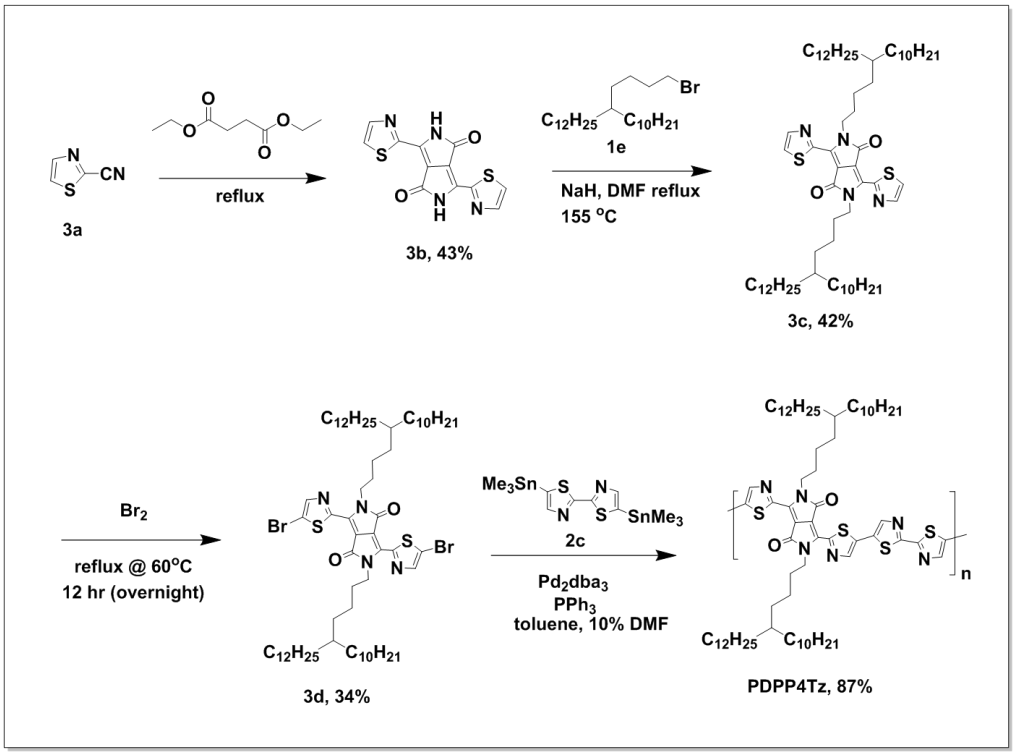

Scheme S1. Synthetic route to prepare **PDPP4Tz**.

Commercially available 2-bromothiazole (**2a**) was homocoupled to afford 2,2'-bithiazole (**2b**)[4], followed by metalation to afford the distannane monomer, 5,5'-bis(trimethylstannyl)-2,2'-bithiazole (**2c**)[5]. Conversion of **2b** to **2c** approached 95% based on ^{1}H NMR analysis. Polymerization was carried out with freshly prepared monomer **2c**.

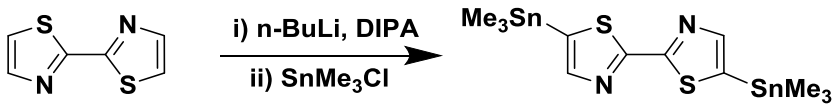

2b **2c, 85%**

5,5'-bis(trimethylstannyl)-2,2'-bithiazole (2c): DIPA (0.45 mL, 3.12 mmol, 3.50 eq.) in THF (2 mL) was maintained under an argon atmosphere and cooled to -78 ˚C using a dry ice/acetone bath. Then, n-butyllithium (1.00 mL of a 2.5 M solution in hexane, 2.50 mmol, 2.80 eq.) was added in a dropwise manner. The resulting solution was then warmed to 0 °C using an ice-water bath and stirred at 0 °C for 30 min to afford lithium diisopropylamide (LDA). It was subsequently cooled to -78 ˚C in dry ice/acetone bath. Then, **2,2'-bithiazole** (150 mg, 0.9 mmol, 1.00 eq.) in THF (3.9 mL) was added in a dropwise manner generating an orange solution. After stirring at -78 ˚C for 2 h, $SnMe_3Cl$ (3.25 mL of a 1.0 M solution in THF, 3.25 mmol, 3.64 eq.) was added in a dropwise manner. The resulting solution was then warmed to room temperature and stirred for 12 h. The solution was then poured into D.I. H_2O (50 mL), the mixture was extracted into CH_2Cl_2 (3 × 15 mL), washed with brine (3 × 15 mL), dried over anhydrous $MgSO_4$, filtered and then concentrated under reduced pressure using a rotary evaporator. The final product was washed with hexane at -78 ˚C and compound **1** was isolated as a pale yellow solid (370 mg, yield: 85%). ^{1}H NMR (400 MHz, $CDCl_3$) δ 7.77 (s, 2H), 0.41 (s, 18H).

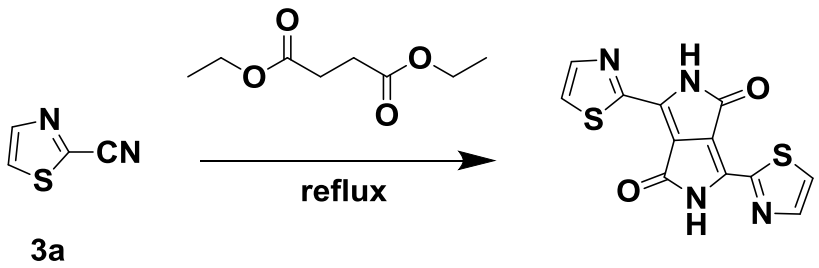

3a

3b, 43%

Synthesis of 3,6-Bis-thiazol-2-yl-2,5-dihydro-pyrrolo[3,4-c]pyrrole-1,4-dione (13). 1.00 g of sodium metal were diced and carefully added into a 2-neck round bottom flask fit with a condenser. 40 mL of t-amyl alcohol was added in the flask with a stirrer. The reaction mixture was heated then overnight at 125 ^{o}C. 2.22 g (2.12 mL, 12.8 mmol) of diethyl succinate and 2.0 g (18.2 mmol) of **3a** were added into to 20 mL of t-amyl alcohol, then slowly added dropwise. The reaction mixture was then stirred at 110 ^{o}C for 8 hours. Mixture was cooled to room temperature afterwards, and the product was precipitated by pouring slowly into a mixture of 4.0 g glacial acetic acid, 100 mL of water, and 50 mL of methanol. The product was then filtered and washed with methanol followed by drying in a vacuum oven at 45 ^{o}C overnight to yield the product as a purple solid (1.18 g, 43%). MALDI-TOF calculated m/z = 301.99, found m/z = 301.47.

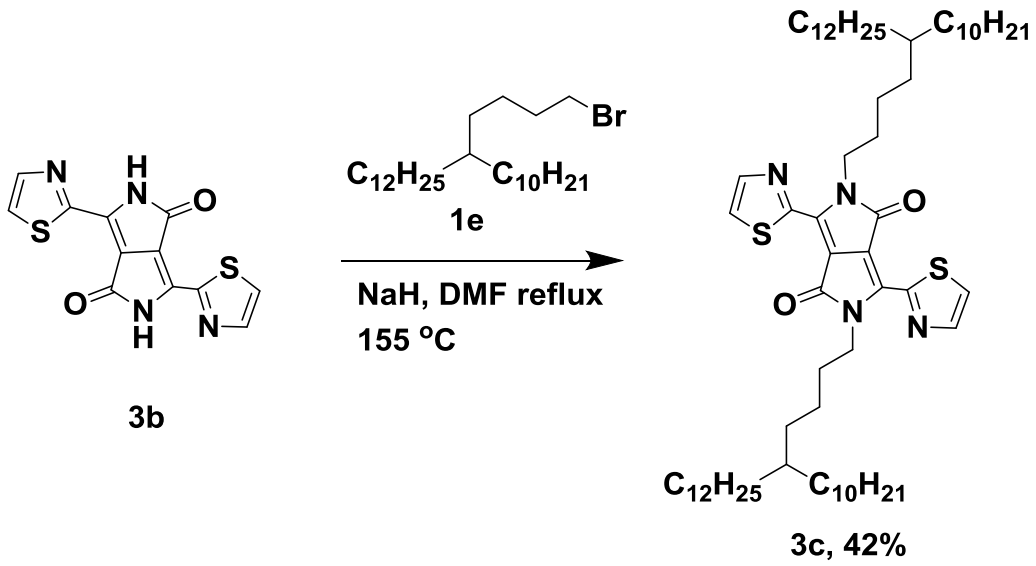

2,5-bis(5-decylheptadecyl)-3,6-di(thiazol-2-yl)-2,5-dihydropyrrolo[3,4-c]pyrrole-1,4-dione (3c): **1e** (6.08 g, 13.23 mmol, 4.00 eq.) was added into the mixture of **3b** (1.00 g, 3.30 mmol, 1.00 eq.) and a 60% mineral oil suspension of NaH (0.39 g, 9.75 mmol) in anhydrous DMF (40 mL) under argon. The mixture was heated at reflux for 24 h, before cooling to room temperature. D.I. H_2O (100 mL) was added and the mixture was extracted into $CHCl_3$ (50 mL). The organic solution was washed with brine (3 × 50 mL), dried over anhydrous $MgSO_4$, and concentrated under reduced pressure. The resulting dark residue was purified by column chromatography (silica gel, DCM). The product was recrystallized from isopropanol to afford **3c** as a purple solid (yield: 42 %). ^{1}H NMR (400 MHz, $CDCl_3$) δ: 8.07 (d, J = 2.4 Hz, 2H), 7.70 (d, J = 1.6, 2H), 4.40 (m, 4H), 1.68 (m, 4H), 1.32–1.19 (m, 90H), 0.87 (t, J = 6.8 Hz, 12H). ^{13}C NMR (400 MHz, $CDCl_3$) δ (ppm): 160.9, 155.3, 144.4, 137.6, 123.9, 110.5, 42.9, 37.3, 35.6, 33.3, 31.9, 30.2, 29.7, 26.2, 24.0, 22.7, 14.1. MALDI-TOF: calculated m/z = 1058.84, found 1057.71.

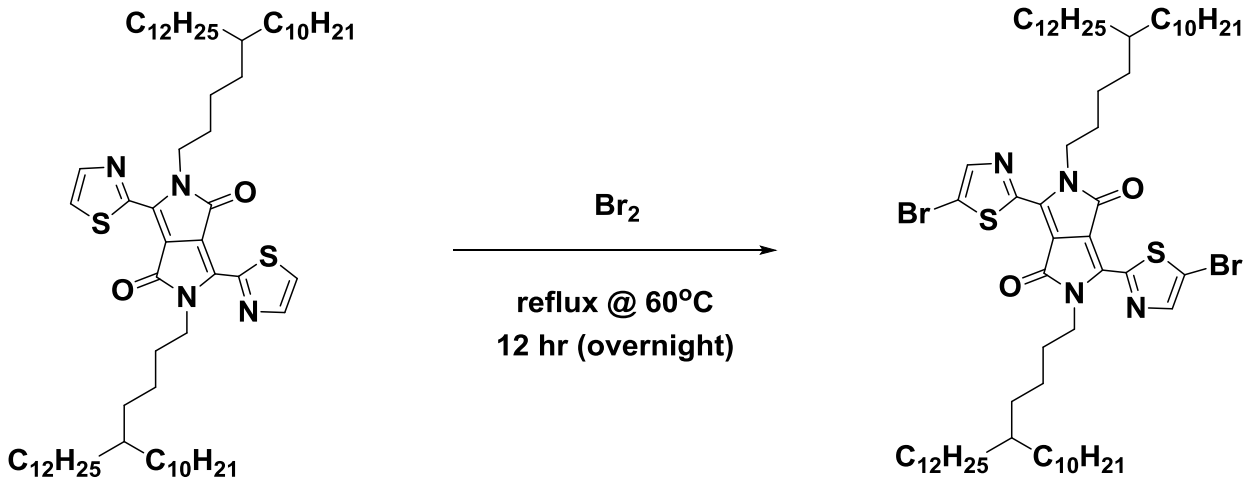

3c **3d, 34%**

3,6-bis(5-bromothiazol-2-yl)-2,5-bis(5-decylheptadecyl)-2,5-dihydropyrrolo[3,4-c]pyrrole-1,4-dione (3d): Sodium bicarbonate (0.435 g, 5.17 mmol) was added into a solution of **3c** (0.5 g, 0.47 mmol) in $CHCl_3$ (9 mL). A solution of Br_2 (0.75 g, 4.72 mmol) in $CHCl_3$ (9 mL) was added during a course of 20 min at 0 °C. The reaction mixture was stirred at 60 °C for 2 hr, followed by cooling to room temperature. A sodium thiosulfate solution (5.0 g in 20 mL H_2O) was added into the reaction mixture and stirred for 30 min to remove residual Br_2. The mixture was washed with brine (50 mL), followed by drying over anhydrous $MgSO_4$. The resulting solid was subjected to column chromatography (silica, eluent heptane/$CHCl_3$, v/v 60:40) to afford **3d** as titled product. The solid was dissolved in $CHCl_3$ (5 mL) and precipitated into methanol (100 mL) to afford pure **3d** (0.32 g, 34 %) as a red solid. ^{1}H NMR (400 MHz, $CDCl_3$) δ (ppm): 7.93 (s, 2H), 4.31 (d, 4H), 1.65 (m, 2H), 1.50-1.20 (m, 90H), 0.87 (m, 12H). ^{13}C NMR (400 MHz, $CDCl_3$) δ (ppm): 160.7, 156.3, 136.6, 115.9, 110.7, 42.9, 37.3, 33.3, 30.2, 29.7, 26.7, 22.7, 14.1. MALDI-TOF: calculated m/z = 1216.66, found 1215.43.

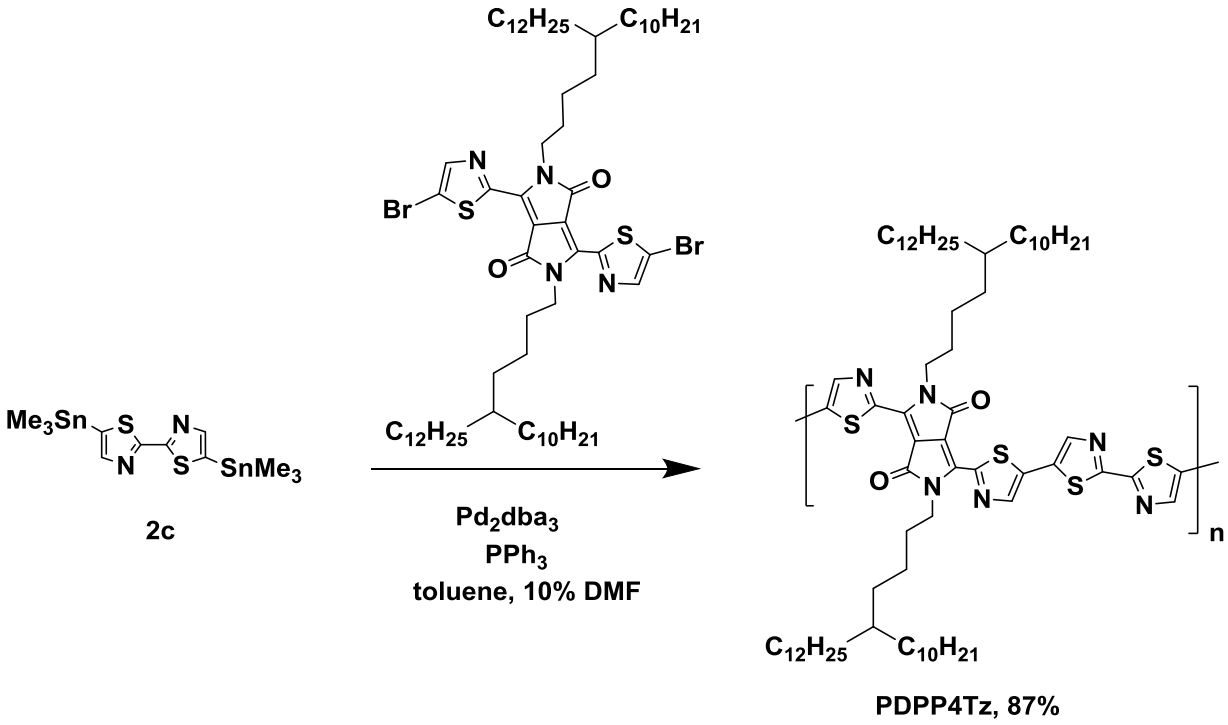

Polymer PDPP4Tz: To a degassed solution of monomer **3** (94.97 mg, 0.078 mmol), 5,5´- 5,5'-bis(trimethylstannyl)-2,2'-bithiazole (**4**) (38.5 mg, 0.078 mmol) in toluene (2 mL) and DMF (0.2 mL), tris(dibenzylideneacetone)dipalladium(0) (2.11 mg, 2.3 µmol) and triphenylphosphine (2.44 mg, 9.3 µmol) were added. The mixture was stirred at 115 °C for 16 h, after which it was precipitated in methanol and filtered through a Soxhlet thimble. The polymer was extracted sequentially with acetone (24 hr), MeOH (24 hr), hexane (24 hr) and dichloromethane (12 hr), and then dissolved in chloroform. The chloroform solution was then precipitated into MeOH. Finally, the resulting polymer can be solubilized in chloroform and xylene for physical property characterization and device fabrication. Yield: 85.4 mg (87%) as a dark blue-green solid. ^{1}H NMR (400 MHz, $CDCl_3$) δ (ppm): 7.99, 7.89, 3.67, 1.51, 1.17, 0.80. Elemental analysis: calculated: C, 70.88%; H, 9.65%; N, 6.70%; found: C, 70.85%; H, 9.52%; N, 6.56%.

UV-vis spectrum of PDPP4Tz

The broader thin film absorption in the range of 750-770 nm suggests the probable self-assembly of **PDPP4Tz** into ordered aggregates that experience enhanced π-π intermolecular interactions[2]. A weak shoulder at ~765 nm in the solution spectra suggests that aggregates also form in the solution phase. Such low band-gap polymers have been found to enhance intramolecular charge transfer, which in turn improves charge carrier mobility [6-9].

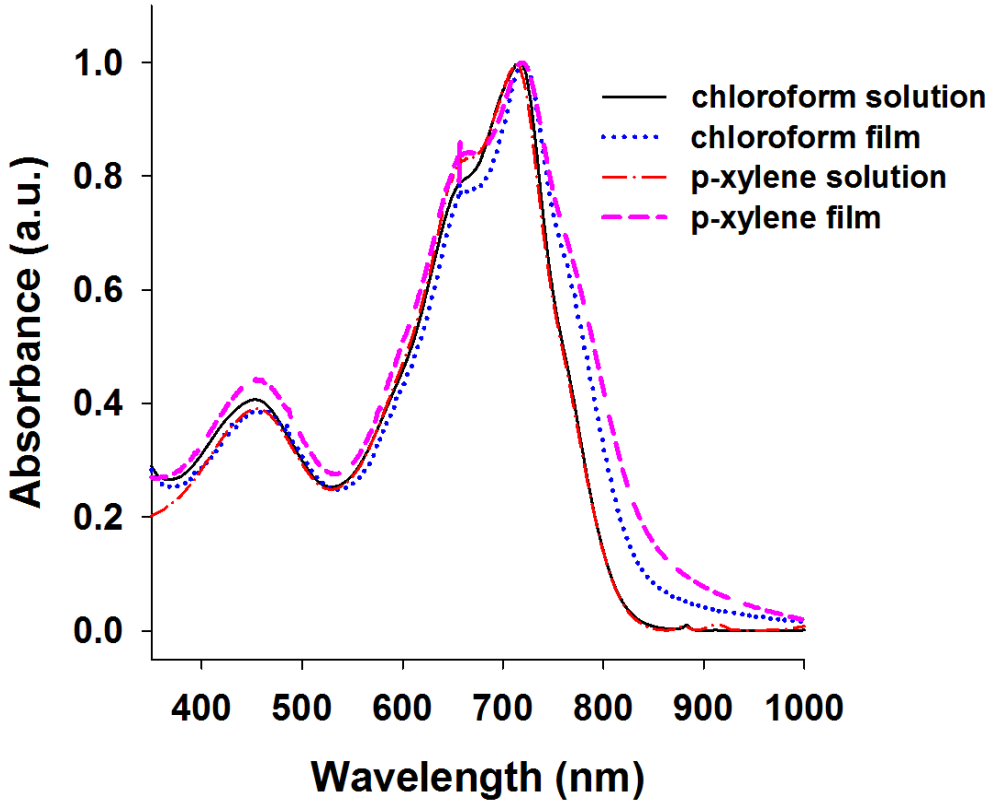

Figure S1. UV-vis absorption spectra of **PDPP4Tz** in solution and thin-film state (1×10^{-6} M; chloroform, p-xylene). Film UV-vis spectra were obtained by spincoating solutions onto UV-ozone cleaned SiO_2 slides before thermal annealing.

TGA and DSC of PDPP4Tz

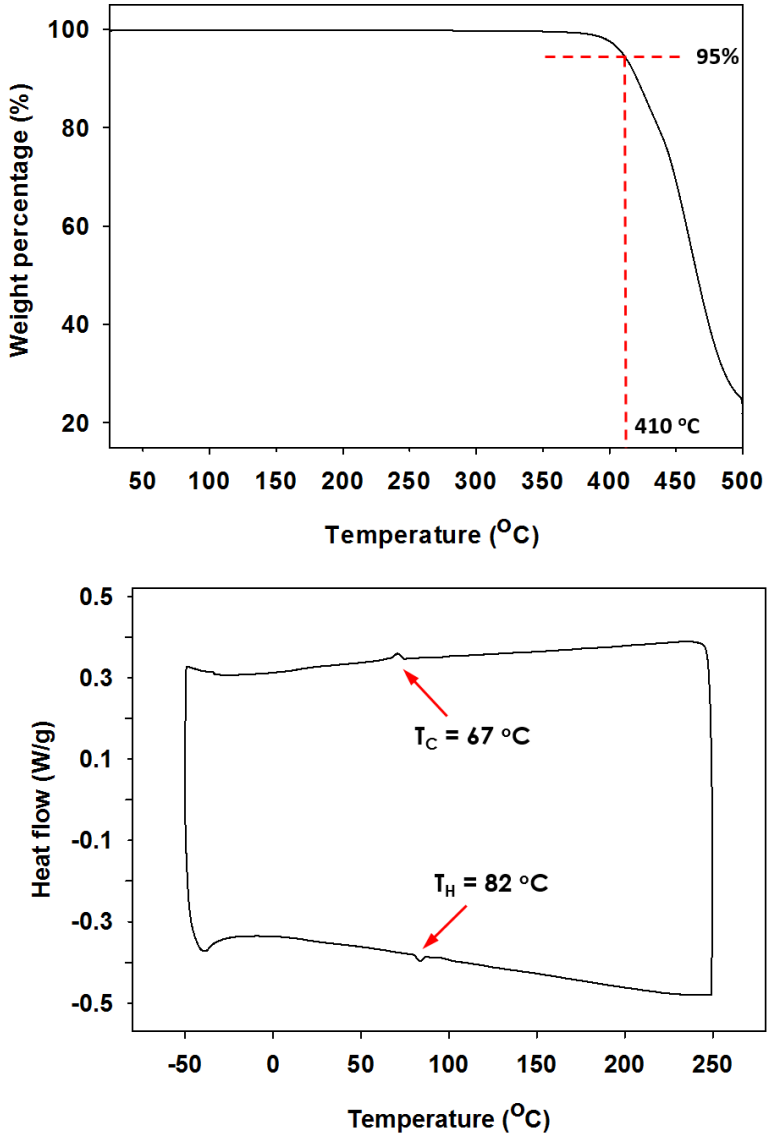

Figure S2. (top) TGA of polymer **PDPP4Tz** in a nitrogen atmosphere (25 mL/min) at a heating rate of 5 °C/min; (bottom) thermal transition characterization of **PDPP4Tz**. DSC characterization was based on the 2nd heating and cooling process in a nitrogen atmosphere with a nitrogen flow rate of 50 mL/min and a heating/cooling rate of 5 °C/min.

^{1}H and ^{13}C NMR spectra of PDPP4Tz

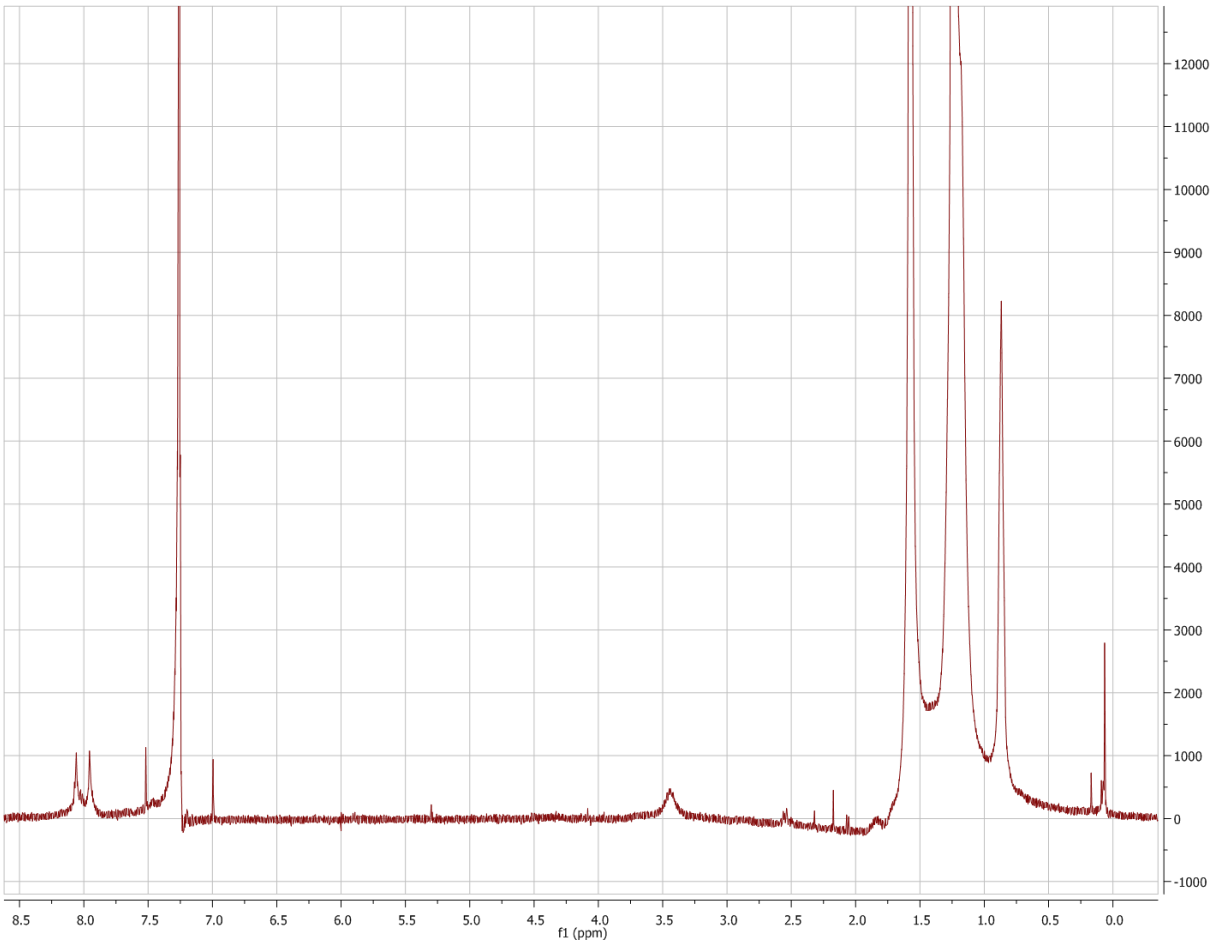

Figure S3. ^{1}H NMR spectrum of **PDPP4Tz** in $CDCl_3$.

DFT studies of PDPP4Tz oligomers and their subunits

The DFT calculations of the oligomers of **PDPP4Tz** were performed using Gaussian 09.[10] We have considered the long-range corrected tuned-ωB97X-D functional along with 6-31G(d,p) basis set for the time-dependent density functional theory *(*TDDFT) calculations; the IP-tuning procedure[11, 12] is carried out with chloroform taken as the dielectric medium (ε = 4.71) to be consistent with experiment, within the self-consistent reaction field (SCRF) framework, to calculate the range separation parameter (ω). The optical gap of the **PDPP4Tz** oligomers levels off at 4 repeat units (**Figure S4**); it corresponds to 1.74 eV at this oligomer size, which is close to the experimental optical gap of 1.72 eV estimated from the UV−vis absorption maxima in chloroform (experimental optical gap evaluated from the onset of absorption is *ca*. 1.34 eV).

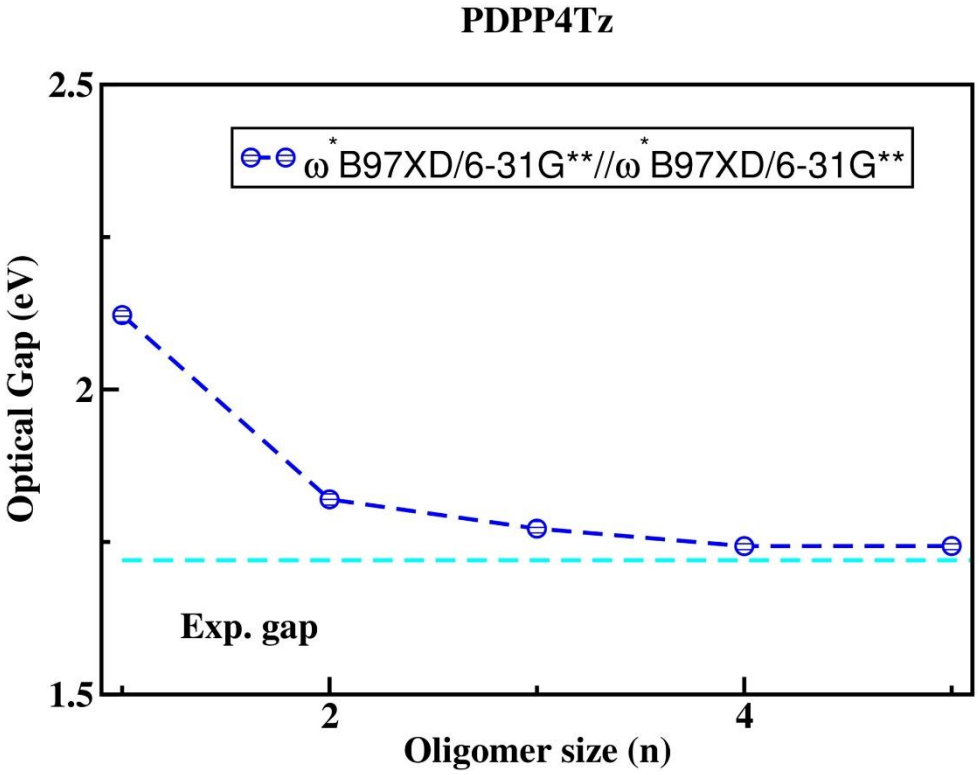

Figure S4. Evolution of the TD-DFT calculated optical band gap vs. oligomer size at the tuned-ωB97X-D/6-31G(d,p)//tuned-ωB97X-D/6-31G(d,p) level of theory.

The dominant natural transition orbital (NTO) of the **PDPP4Tz** tetramer for the S_0 to S_1 transition, at tuned-ωB97X-D/6-31G(d,p) level of theory, is well delocalized along the polymer backbone for both hole and electron (see **Figure S5**); the spin density for the unpaired electron corresponding to the electron-polaron (anion) of the **PDPP4Tz** tetramer is calculated to be delocalized over one full repeat unit, or about 8 to 10 rings (**Figure S6**).

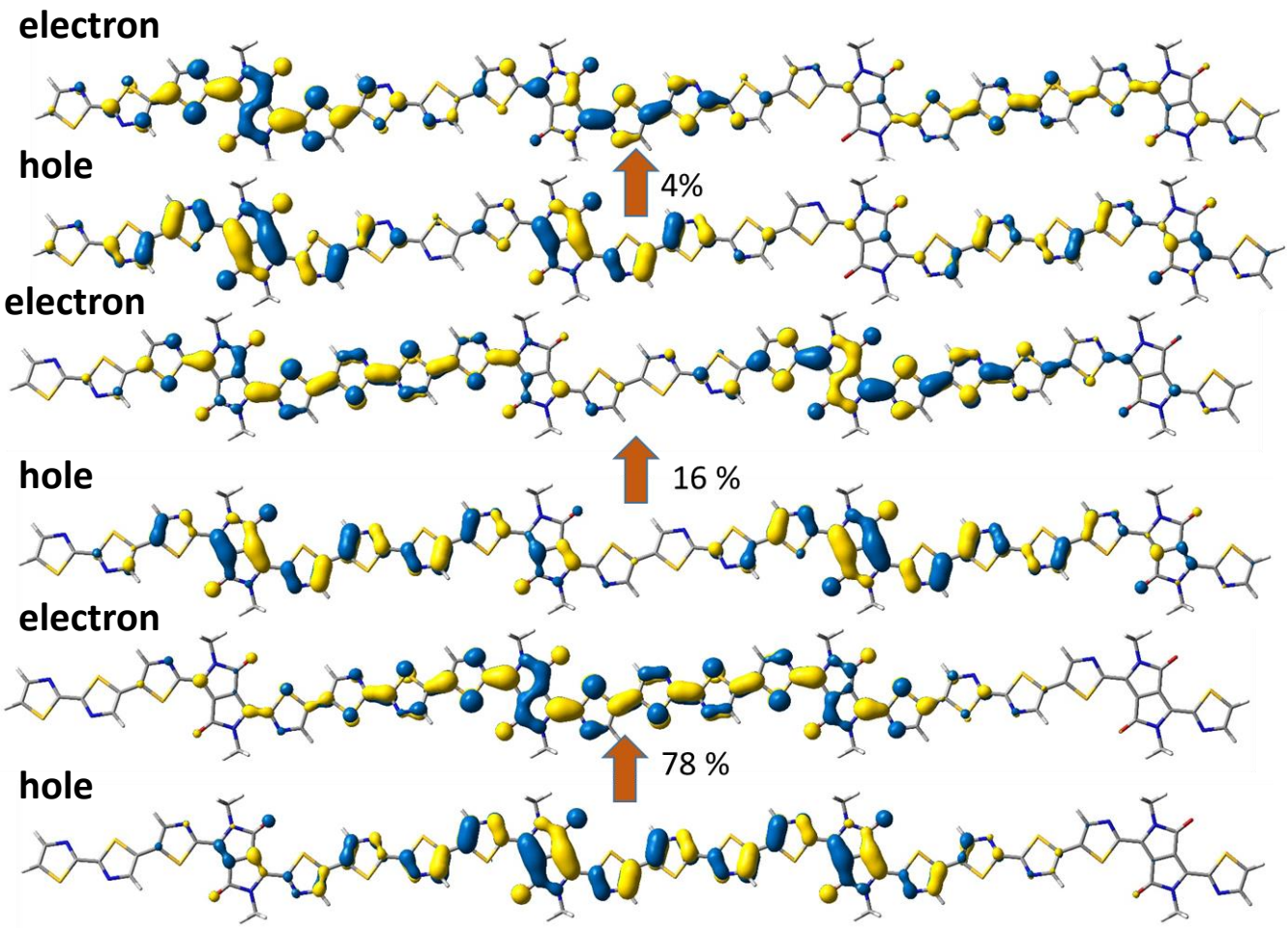

Figure S5. Electron-hole pair natural transition orbitals (isovalue surface 0.02 a.u.) for the S_0 to S_1 transition of the **PDPP4Tz** tetramer calculated by TD-DFT at tuned-ωB97X-D/6-31G(d,p) level of theory. The weights of the particle-hole contribution to the excitation are included.

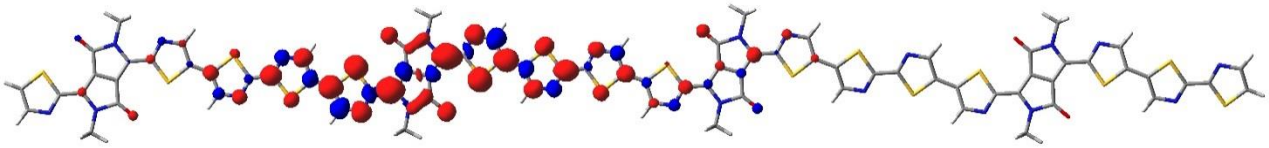

Figure S6. Tuned-ωB97X-D spin density plots for the anion of the **PDPP4Tz** tetramer (the red and blue colors represents spin up and spin down electron densities, respectively).

The electronic band structure of the polymer chain has been modeled using the CRYSTAL14 code.[13] In that instance, the polymer geometry was optimized at the B3LYP level,[14] and the electronic band structure calculated at the HSEsol functional level.[15] The Peintinger-Oliveira-Bredow triple-ζ valence plus polarization (POB-TZVP) basis set[16] using 2k points as set by the Pack-Monkhorst method,[17] was considered for all these calculations. The effective mass for the polymer chain was calculated at the bottom of the conduction band using the band fitting method.[18]

The band structure of the **PDPP4Tz** polymer is shown in **Figure S6**. The band gap of the **PDPP4Tz** polymer is calculated here to be 1.32 eV. The effective mass of an electron (at the bottom of the conduction band) and hole (at the top of the valence band) are calculated (See Table S1).

Table S1. Calculated valence band (VB) width, conduction band (CB) width, band gap, and hole and electron effective masses for the **PDPP4Tz** polymer.

Polymer	Width of VB (eV)	Width of CB (eV)	Band Gap (eV)	m_h/m_0	m_e/m_0
PDPP4Tz	0.25	0.34	1.32	0.18	0.15

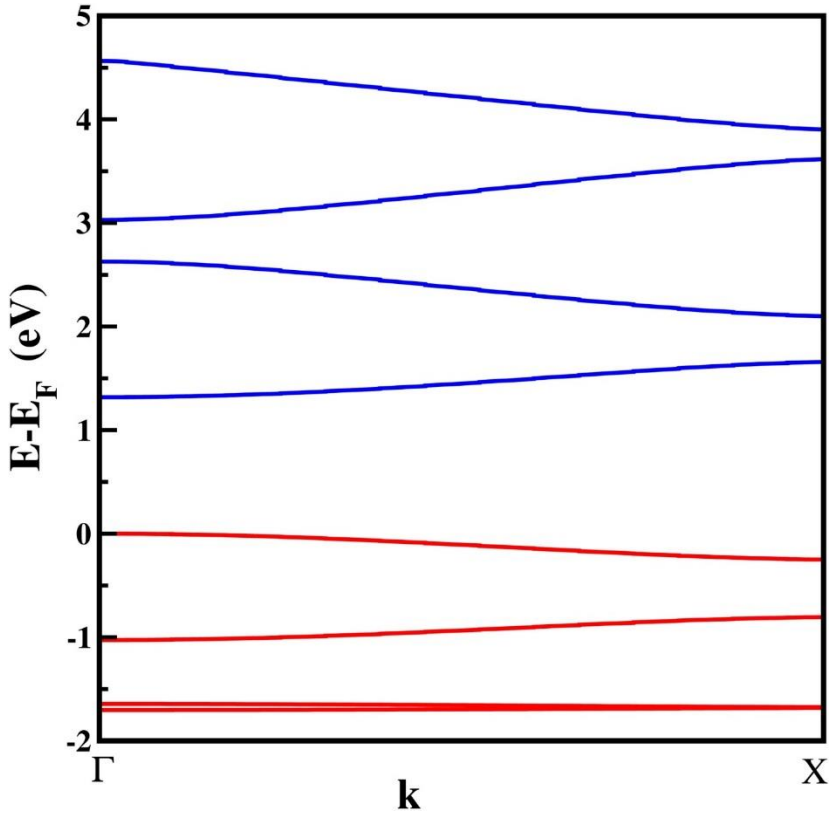

Figure S7. HSEsol//B3LYP electronic band structure of the **PDPP4Tz** chain. The zero of energy corresponds here to the top of the valence band.

UPS spectra of PDPP4Tz

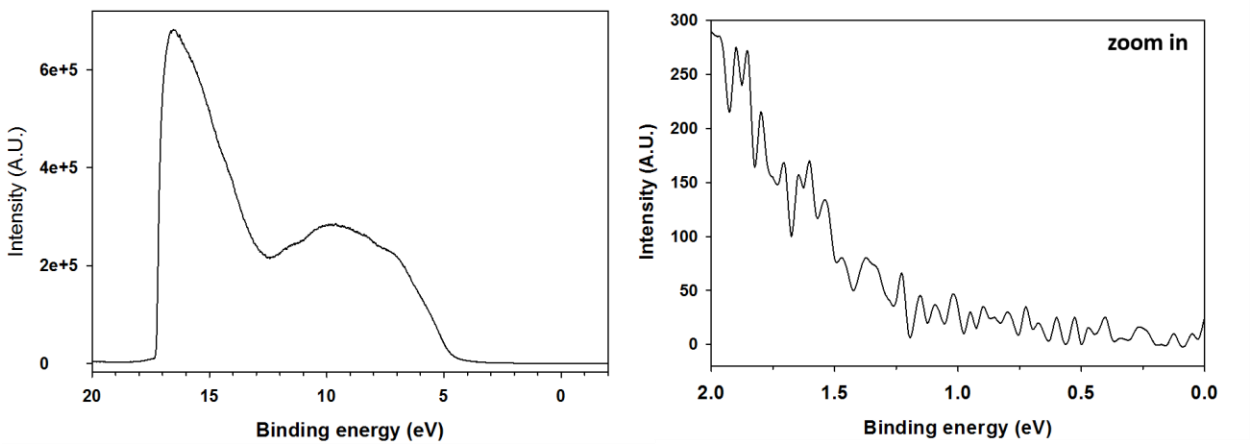

Figure S8. (left) UPS characterization of as-spun **PDPP4Tz** film on gold-coated Si wafer; (right) zoomed-in of lower binding energy region of the UPS spectrum.

Ultraviolet Photoemission Spectra (UPS) were measured on a Kratos Axis UltraDLD XPS/UPS system, using He-I lamp radiation at 21.2 eV. All samples were in electronic equilibrium with the spectrometer via a metallic clip on the surface, and were run at a base pressure of 10^{-5} Torr. The Fermi level was calibrated using atomically clean silver. UPS were acquired at a 5 eV pass energy and 0.05 eV step size with the aperture and iris set to 55 μm. From S4 the secondary electron edge (SEE) of the UPS the work function (ϕ = 21.22-SEE) was calculated for each polymer, and from the emission close to the Fermi level the position of valence band maximum was determined. IP (= –HOMO) and ϕ were calculated by equations (1) and (2):

$$IP = h\upsilon - \left(E_{cutoff} - \varepsilon_V^F\right) \quad (1)$$

$$\phi = h\upsilon - E_{cutoff} \quad (2)$$

where $h\upsilon$, E_{cutoff}, and ε_V^F denote the incident photo energy (He I, 21.22 eV), the high binding energy cutoff, and the lowest binding energy point, respectively.

Molecular weight distribution by GPC

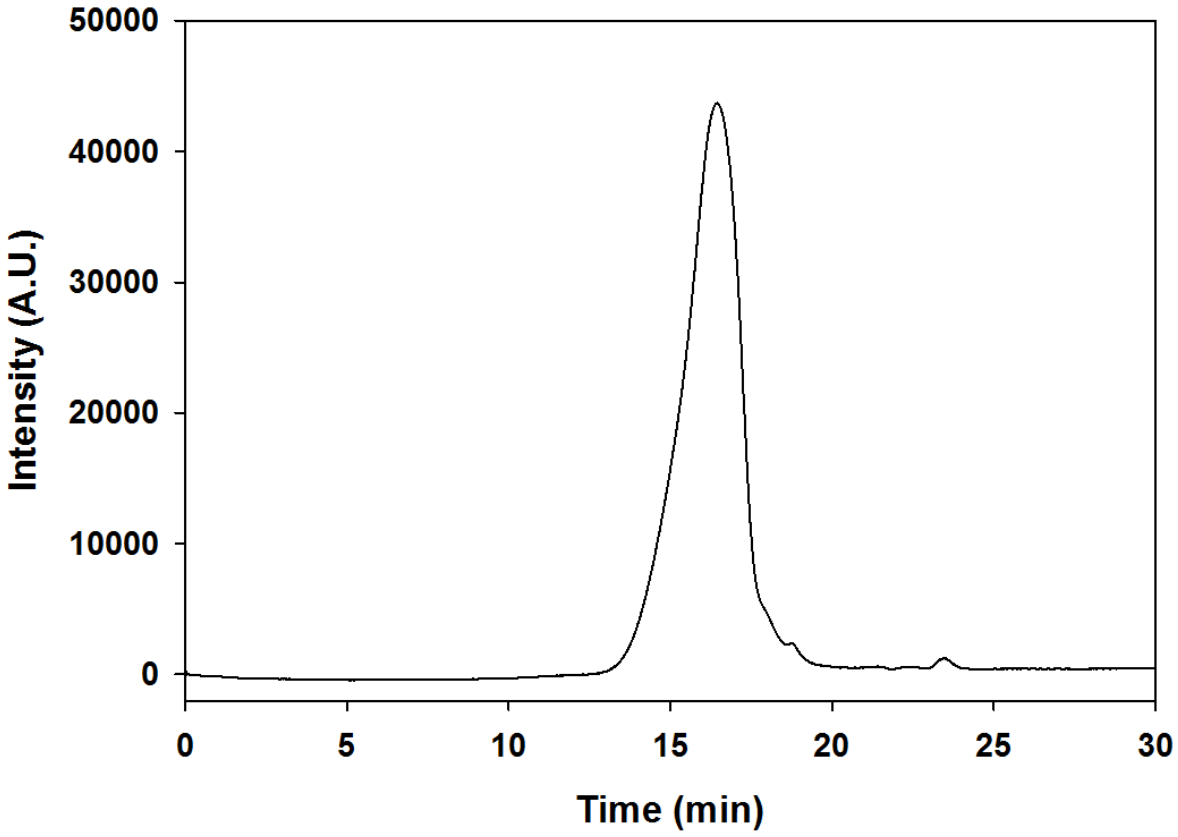

Peak#	Mn	Mw	Mz	Mz1	Mw/Mn	Mz/Mw
Total	26391	35687	51173	91104	1.35222	1.43395
1	26391	35687	51173	91104	1.35222	1.43395

Figure S9. Gel permeation chromatography (GPC) characterization of **PDPP4Tz** with TCB under 135 ^{o}C.

1D X-ray scattering spectrum of PDPP4Tz thin films

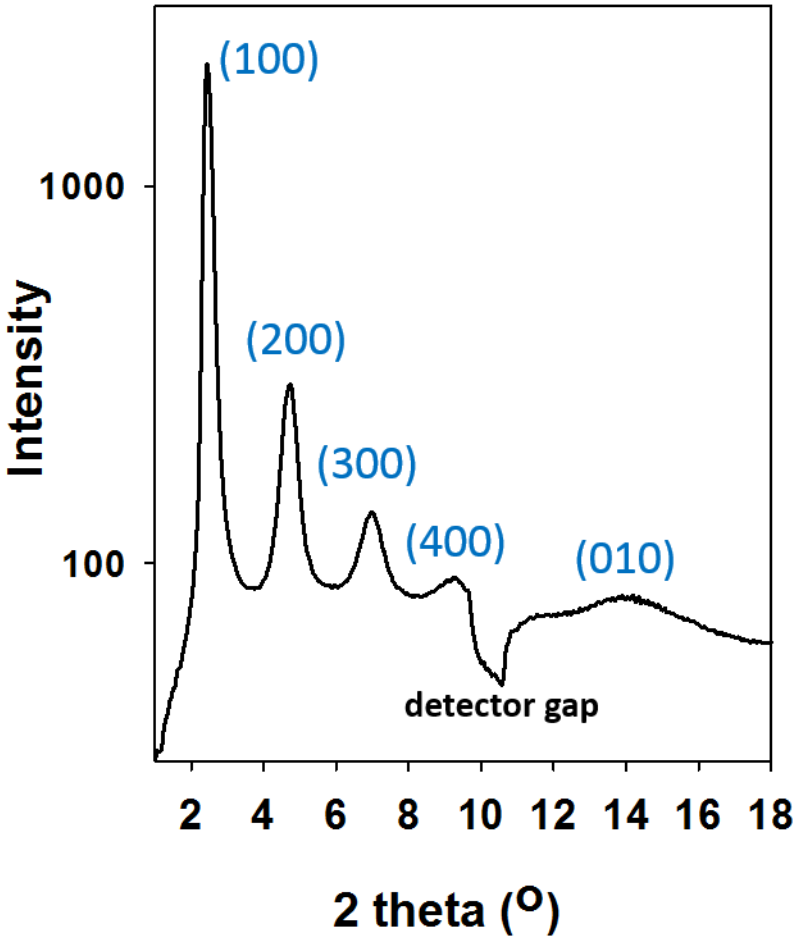

Figure S10. 1D-GIXS patterns of **PDPP4Tz** thin films. Films were spin cast at room temperature in a nitrogen filled glove box from a chloroform solution.

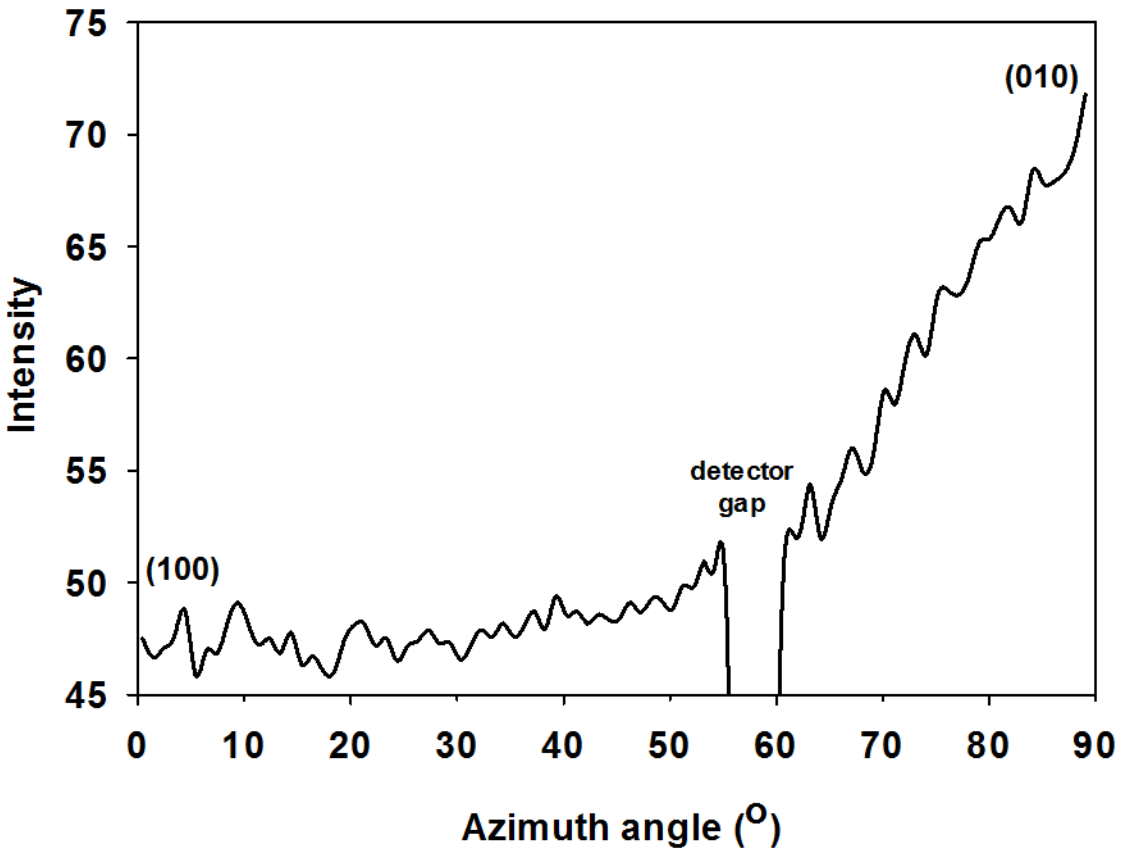

Figure S11. The intensity variation of the (010) peak at (2θ =18-19^{o}) along the γ axis from out-of-plane, q_z (100) to in-plane, q_{xy} (010) measured from a **PDPP4Tz** thin film cast by spincoating from p-xylene solution followed by thermally annealing at 150 ^{o}C for 90 min in a nitrogen filled glovebox.

Birefringence

Given the importance of molecular order in determining the charge transport characteristics in π-conjugated polymers, **PDPP4Tz** exhibits anisotropy within thin films fabricated with blade-coating, as observed under polarized optical microscopy (**Figure S12**). Thin films were cast from both filtered **PDPP4Tz** chloroform and p-xylene solutions (4~6 mg/mL) onto UV-ozone cleaned glass slides at room temperature. The observed birefringence indicates that **PDPP4Tz** polymer chains adopt a highly self-organized morphology, which allows the chains to form ordered anisotropic domains in thin-films. As intermolecular charge transport across grain boundaries, or through disordered domains is not as efficient as within ordered domains, increasing the grain size is expected to be a favorable approach to increase charge-carrier mobility.

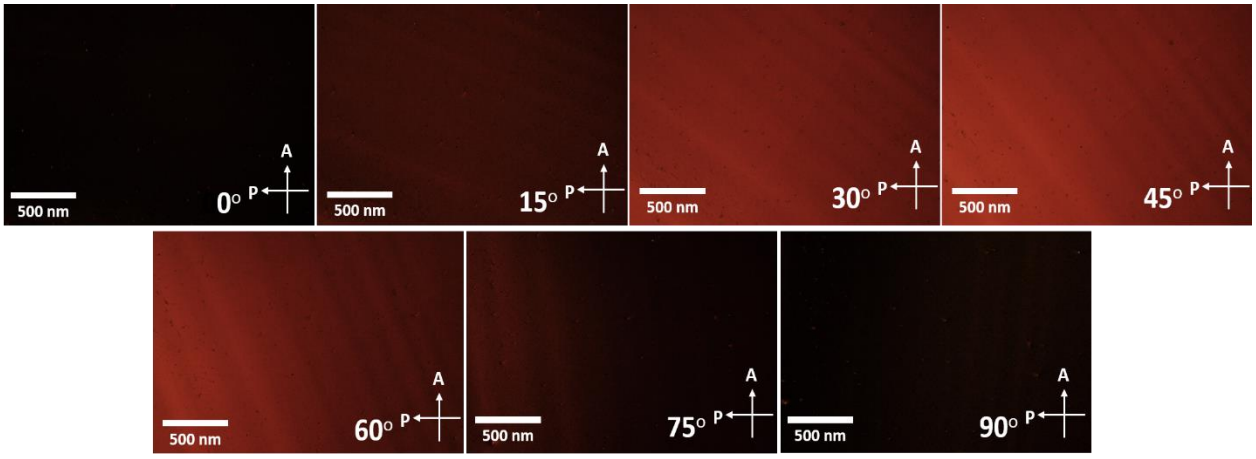

Figure S12. Polarized Optical Microscope (POM) images of blade-coated **PDPP4Tz** films on glass slides (chloroform as solvent).

Atomic Force Microscope Image of PDPP4Tz Thin Film

PDPP4Tz thin-film surface morphologies were investigated using tapping mode atomic force microscopy (AFM) as shown in **Figure S13**. Polymer films were spin-cast and blade-coated onto OTS-18 functionalized SiO_2 on Si substrates. All blade-coated polymer films exhibited consistent surface morphology patterns, appearing highly ordered with a feathery-like texture. The annealed films appeared with a nano-granular character, which is consistent with the high crystallinity revealed by GIWAXS.

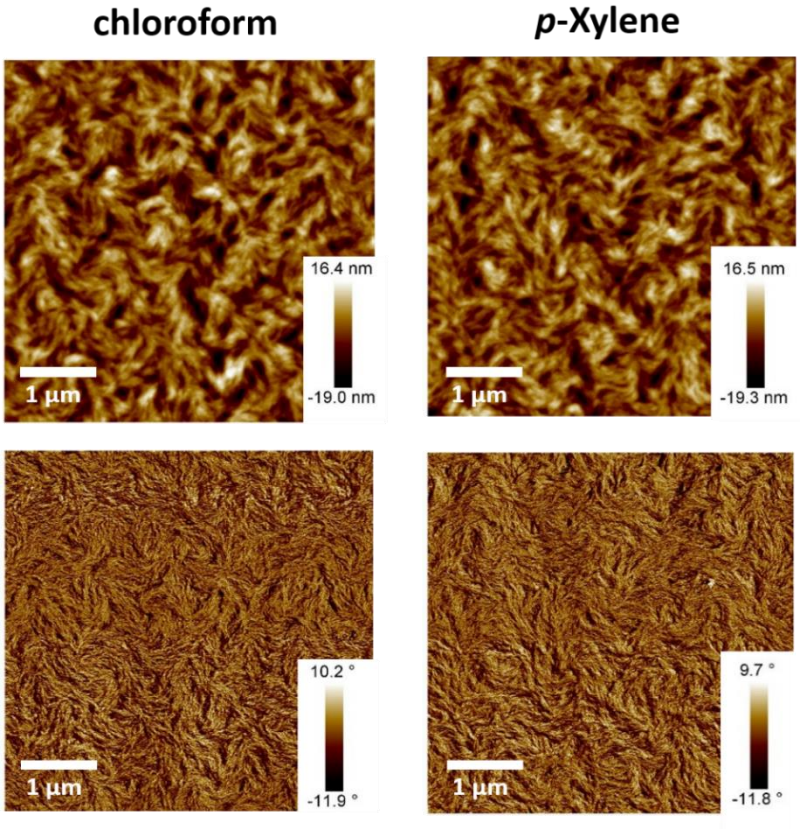

Figure S13. Tapping mode AFM height (top row) and phase (bottom row) images of **PDPP4Tz** blade coated films recorded after thermal annealing each film at 150 ^{o}C for 90 min followed by rapid cooling to room temperature in a nitrogen filled glove box.

OFET Device Fabrication and Characterization

BG/BC OFETs were fabricated on a heavily *p* doped silicon wafer <100> as the gate electrode with a 300 nm thick layer of thermally grown SiO_2 as the gate dielectric. Au source and drain contacts (50 nm of Au contacts with 3 nm of Cr as the adhesion layer) with fixed channel dimensions (50 μm in length and 2 mm in width) were deposited via E-beam using a photolithography lift-off process. Prior to deposition of polymer semiconductors, the devices were cleaned in acetone for 30 min and subsequently rinsed sequentially with acetone, methanol and isopropanol. The SiO_2 surface was pretreated by UV/ozone for 30 min followed by immersion into a 2.54 x 10^{-3} M (1 μL mL^{-1}) solution of OTS-18 in anhydrous toluene. The devices were then cleaned by sonication in toluene for 10 min, followed by rinsing sequentially with acetone, methanol and isopropanol, and drying under a flow of nitrogen. The H_2O contact angle for the SiO_2 surface after OTS-18 treatment was in the range of 95–105°; the OTS-18 modified SiO_2 dielectric has a capacitance of *ca*. 1.1 x 10^{-4} Fm^{-2}. **PDPP4Tz** solutions were then spin-coated onto substrates inside a N_2 filled glovebox or blade coated in ambient condition.

The capacitances of the dielectric layers were measured using an Agilent 4284A Precision LCR Meter. All OFET characterizations were performed using a probe station inside a nitrogen filled glovebox using an Agilent 4155C semiconductor parameter analyzer. The FET mobilities were calculated from the saturation regime in the transfer plots of V_G versus I_{SD} by extracting the slope of the linear range of V_G vs. $I_{SD}^{1/2}$ plot and using the following equation:

$$\frac{\partial I_{SD}^{1/2}}{\partial V_G} = (\mu_e C_{ox} \frac{W}{2L})^{1/2} \qquad (3)$$

where I_{SD} and V_{SD} are the source-drain current (A) and source-drain voltage (V), respectively; V_G is the gate voltage (V) scanning from -20 to 80 V (for BGBC OFETs) in the transfer plot; C_{ox} is

the capacitance per unit area of the gate dielectric layer. *W* and *L* refer to the channel length and width; μ_e represents the electron field-effect mobility in the saturation regime ($cm^2V^{-1}s^{-1}$).

In this study, the threshold voltage, V_{th}, was calculated by extrapolating $V_T = V_G$ at $I_{SD} = 0$ in the V_G vs. $I_{SD}^{1/2}$ curve. Current on/off ratio, $I_{ON/OFF}$, was determined through dividing maximum I_{SD} (I_{ON}) by the minimum I_{SD} at about V_G in the range of -20 to 0 V (I_{OFF}). It is noted that **PDPP4Tz** field-effect mobility was more stable and hysteresis was reduced after thermal annealing at 150 °C for 90 min in OFETs and no obvious improvement was observed at annealing temperatures above 150 °C. The thermal annealing treatment was hence fixed at 150 °C for 90 min.

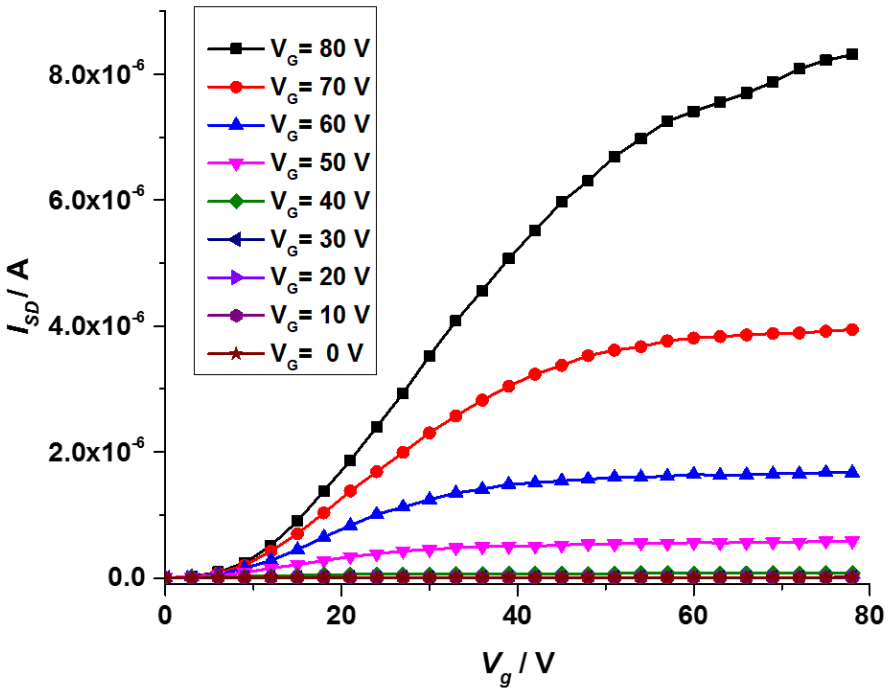

Figure S14. Output characteristics of the bottom-gate/bottom-contact (BG/BC) transistors fabricated by spincoating p-xylene solution of **PDPP4Tz**

Stability Study

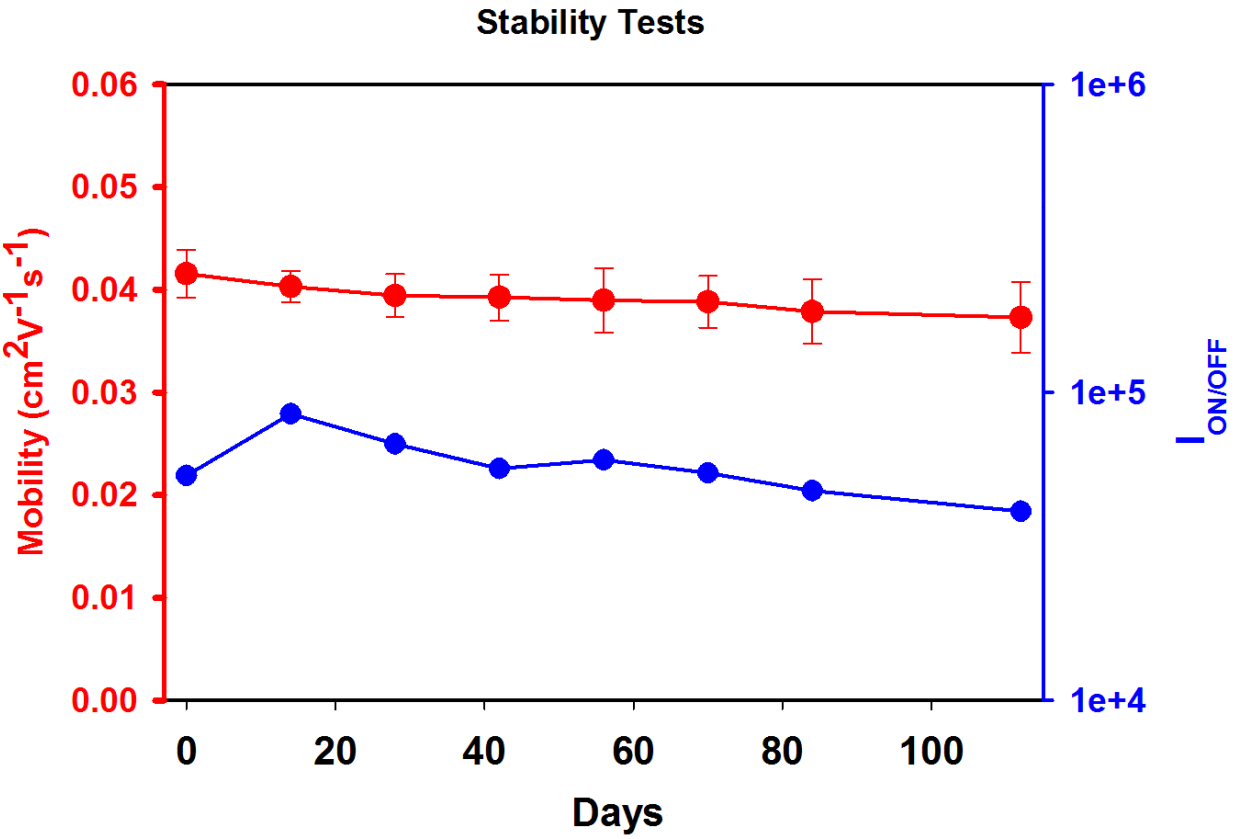

Figure S15. Effect of OFET stability under ambient conditions (25 ^{o}C and 50-60% RH). Devices are fabricated on Si-wafers based on the BGBC configuration. Mobility data were measured in a nitrogen filled glovebox with devices stored in vacuum chamber for 12 hours to remove moisture and residual air.

References:

(1) Fu, B.; Baltazar, J.; Sankar, A. R.; Chu, P.-H.; Zhang, S.; Collard, D. M.; Reichmanis, E. Enhancing Field-Effect Mobility of Conjugated Polymers Through Rational Design of Branched Side Chains *Adv. Funct. Mater.* **2014,** *24*, 3734-3744.

(2) Fu, B.; Wang, C.-Y.; Rose, B. D.; Jiang, Y.; Chang, M.; Chu, P.-H.; Yuan, Z.; Fuentes-Hernandez, C.; Kippelen, B.; Brédas, J.-L.; Collard, D. M.; Reichmanis, E. Molecular Engineering of Nonhalogenated Solution-Processable Bithiazole-Based Electron-Transport Polymeric Semiconductors *Chem. Mater.* **2015,** *27*, 2928-2937.

(3) Li, W.; Roelofs, W. S. C.; Turbiez, M.; Wienk, M. M.; Janssen, R. A. J. Polymer Solar Cells with Diketopyrrolopyrrole Conjugated Polymers as the Electron Donor and Electron Acceptor *Adv. Mater.* **2014,** *26*, 3304-3309.

(4) Hassan, J.; Lavenot, L.; Gozzi, C.; Lemaire, M. A convenient catalytic route to symmetrical functionalized bithiophenes *Tetrahedron Lett.* **1999,** *40*, 857-858.

(5) Wolf, M. O.; Wrighton, M. S. Tunable Electron Density at a Rhenium Carbonyl Complex Coordinated to the Conducting Polymer Poly[5,5'-(2-thienyl)-2,2'-bithiazole] *Chem. Mater.* **1994,** *6*, 1526-1533.

(6) Ando, S.; Nishida, J.-i.; Tada, H.; Inoue, Y.; Tokito, S.; Yamashita, Y. High Performance n-Type Organic Field-Effect Transistors Based on π-Electronic Systems with Trifluoromethylphenyl Groups *J. Am. Chem. Soc.* **2005,** *127*, 5336-5337.

(7) Karikomi, M.; Kitamura, C.; Tanaka, S.; Yamashita, Y. New Narrow-Bandgap Polymer Composed of Benzobis(1,2,5-thiadiazole) and Thiophenes *J. Am. Chem. Soc.* **1995,** *117*, 6791-6792.

(8) Lee, B.-L.; Yamamoto, T. Syntheses of New Alternating CT-Type Copolymers of Thiophene and Pyrido[3,4-b]pyrazine Units: Their Optical and Electrochemical Properties in Comparison with Similar CT Copolymers of Thiophene with Pyridine and Quinoxaline *Macromolecules* **1999,** *32*, 1375-1382.

(9) Wang, C.; Dong, H.; Hu, W.; Liu, Y.; Zhu, D. Semiconducting π-Conjugated Systems in Field-Effect Transistors: A Material Odyssey of Organic Electronics *Chem. Rev.* **2012,** *112*, 2208-2267.

(10) Frisch, M. J.; Trucks, G. W.; Schlegel, H. B.; Scuseria, G. E.; Robb, M. A.; Cheeseman, J. R.; Scalmani, G.; Barone, V.; Mennucci, B.; Petersson, G. A.; Nakatsuji, H.; Caricato, M.; Li, X.; Hratchian, H. P.; Izmaylov, A. F.; Bloino, J.; Zheng, G.; Sonnenberg, J. L.; Hada, M.; Ehara, M.; Toyota, K.; Fukuda, R.; Hasegawa, J.; Ishida, M.; Nakajima, T.; Honda, Y.; Kitao, O.; Nakai, H.; Vreven, T.; Montgomery Jr., J. A.; Peralta, J. E.; Ogliaro, F.; Bearpark, M. J.; Heyd, J.; Brothers, E. N.; Kudin, K. N.; Staroverov, V. N.; Kobayashi, R.; Normand, J.; Raghavachari, K.; Rendell, A. P.; Burant, J. C.; Iyengar, S. S.; Tomasi, J.; Cossi, M.; Rega, N.; Millam, N. J.; Klene, M.; Knox, J. E.; Cross, J. B.; Bakken, V.; Adamo, C.; Jaramillo, J.; Gomperts, R.; Stratmann, R. E.; Yazyev, O.; Austin, A. J.; Cammi, R.; Pomelli, C.; Ochterski, J. W.; Martin, R. L.; Morokuma, K.; Zakrzewski, V. G.; Voth, G. A.; Salvador, P.; Dannenberg, J. J.; Dapprich, S.; Daniels, A. D.; Farkas, Ö.; Foresman, J. B.; Ortiz, J. V.; Cioslowski, J.; Fox, D. J. *Gaussian 09, Revision D.01*, Gaussian, Inc.: Wallingford, CT, USA, 2013.

(11) Stein, T.; Kronik, L.; Baer, R. Reliable Prediction of Charge Transfer Excitations in Molecular Complexes Using Time-Dependent Density Functional Theory *J. Am. Chem. Soc.* **2009,** *131*, 2818-2820.

(12) Körzdörfer, T.; Brédas, J.-L. Organic Electronic Materials: Recent Advances in the DFT Description of the Ground and Excited States Using Tuned Range-Separated Hybrid Functionals *Acc. Chem. Res.* **2014,** *47*, 3284-3291.
(13) Dovesi, R.; Orlando, R.; Erba, A.; Zicovich-Wilson, C. M.; Civalleri, B.; Casassa, S.; Maschio, L.; Ferrabone, M.; De La Pierre, M.; D'Arco, P.; Noël, Y.; Causà, M.; Rérat, M.; Kirtman, B. CRYSTAL14: A program for the ab initio investigation of crystalline solids *Int. J. Quantum Chem.* **2014,** *114*, 1287-1317.
(14) Zhao, Y.; Truhlar, D. G. The M06 suite of density functionals for main group thermochemistry, thermochemical kinetics, noncovalent interactions, excited states, and transition elements: two new functionals and systematic testing of four M06-class functionals and 12 other functionals *Theor. Chem. Acc.* **2008,** *120*, 215-241.
(15) Schimka, L.; Harl, J.; Kresse, G. Improved hybrid functional for solids: The HSEsol functional *J. Chem. Phys.* **2011,** *134*, 024116.
(16) Peintinger, M. F.; Oliveira, D. V.; Bredow, T. Consistent Gaussian basis sets of triple-zeta valence with polarization quality for solid-state calculations *J. Comput. Chem.* **2013,** *34*, 451-459.
(17) Monkhorst, H. J.; Pack, J. D. Special points for Brillouin-zone integrations *Phys. Rev. B* **1976,** *13*, 5188-5192.
(18) Hsu, B. B.-Y.; Cheng, C.-M.; Luo, C.; Patel, S. N.; Zhong, C.; Sun, H.; Sherman, J.; Lee, B. H.; Ying, L.; Wang, M.; Bazan, G.; Chabinyc, M.; Brédas, J.-L.; Heeger, A. The Density of States and the Transport Effective Mass in a Highly Oriented Semiconducting Polymer: Electronic Delocalization in 1D *Adv. Mater.* **2015,** *27*, 7759-7765.